APPLICATIONS OF
MODELLING AND SIMULATION
http://arqiipubl.com/ams eISSN 2600-8084 VOL 9, 2025, 349-362

Design and Performance Evaluation of a Novel FOPID Control Strategy for Electric Furnace Temperature Regulation using HHO Algorithm

A. Idir[1,2,*], H. Akroum[2], M. Nesri[3], S. Guedida[4] and L. Canale[5]

[1]Electrical Engineering Department, University Mohamed Boudiaf of M'sila, 28000 M'sila, Algeria
[2]Systems Engineering and Telecommunications Laboratory, University of Boumerdes, 35000 Boumerdes, Algeria
[3]Ecole Supérieur Ali Chabati, Reghaia Algiers, Algeria
[4]Ecole Militaire Polytechnique, UER ELT, 16111 Algiers, Algeria
[5]CNRS, LAPLACE Laboratory, UMR 5213 Toulouse, France

[*]Corresponding author: abdelhakim.idir@univ-msila.dz

Submitted 05 July 2025; Revised 21 August 2025; Accepted 24 August 2025; Available online 15 September 2025.

Abstract: This study introduces the development and implementation of an advanced Proportional-Integral-Derivative (PID) control strategy, termed the Proportional Fractionalized Integral Derivative (PI$^{\alpha}$D) controller, aimed at enhancing transient dynamics, frequency response, and robustness in the regulation of electric furnace temperature. A key feature of the proposed controller design is the incorporation of the Harris Hawks Optimization (HHO) algorithm, employed to optimally tune the controller parameters. The selection of HHO is justified by its superior global search capability, fast convergence, and effectiveness in avoiding local minima, making it well-suited for addressing the complex, nonlinear characteristics of electric furnace systems. The suggested PI$^{\alpha}$D controller is used for the first time in electric furnace applications, providing a novel enhancement to traditional PID controllers by incorporating a fractional-order element. The controller's efficacy is evaluated through stringent simulations encompassing step reference alterations, load disturbances, and continuous random setpoints. Compared to classical PID, PID Acceleration (PIDA), and Real PID with second-order derivative (RPIDD^2) controllers, the proposed PI$^{\alpha}$D controller exhibits superior performance, achieving the fastest rise time (1.65 s), shortest settling time (3.43 s), and lowest overshoot (0.12%). It also provides the best robustness trade-off, with high gain and phase margins, the largest bandwidth, and the lowest error indices. Frequency-domain analysis further confirms its enhanced disturbance rejection and stability, underscoring the suitability of the proposed controller and HHO for accurate, reliable, and energy-efficient temperature regulation in nonlinear industrial systems.

Keywords: Electric furnace; Harris Hawks optimization (HHO); PI$^{\alpha}$D controller design; Temperature control; Stability analysis.

1. INTRODUCTION

Electric furnaces are essential in various industrial areas, transforming electrical energy into heat for processing applications. In these systems, accurate temperature regulation is essential, as insufficient control may result in undesirable alterations or degradation of the material qualities of the treated goods [1]. Ensuring precise accuracy and swift responsiveness in temperature regulation is crucial for sustaining optimal system performance. A variety of control solutions has been presented over the years to effectively address this difficulty. The efficient management of electric furnaces is essential, as it directly impacts the productivity, quality and industrial operations energy efficiency. Accurate temperature control is crucial for attaining the appropriate material characteristics, averting heat-induced deterioration, and maximizing energy efficiency. Inaccurate temperature regulation can result in diminished product quality, elevated energy expenses, and enhanced environmental consequences. Consequently, there is a significant necessity for the ongoing enhancement of control techniques [2-4].

Recent advancements in thermal process control have improved accuracy and robustness through intelligent optimization and advanced control strategies, such as a modified flower pollination algorithm (MOFPA)-based Proportional-Integral-Derivative Acceleration (PIDA) (MOFPA-PIDA) controller [5], fuzzy fractional-order Proportional-Integral-Derivative (PID) controller [6], robust adaptive disturbance rejection control (ADRC) [7], nonlinear model predictive control (MPC) [8], genetic

algorithm-based internal model controller [9] and a particle swarm optimisation (PSO) based Real PID with Second-Order Derivative (RPIDD²) (PSO-RPIDD²) controller [10].

The nonlinear dynamics and time-varying attributes of electric furnace systems make traditional PID controller tuning highly challenging. Consequently, adaptive and intelligent control systems are increasingly favored to guarantee successful regulation. Diverse optimization methodologies have been employed to enhance PID controllers in these contexts, encompassing the Nelder-Mead method [11], fuzzy logic (FL) [12], extended non-minimal state space fractional-order model predictive control (EnMSSFMPC) [13], neural networks [14], enhanced whale optimization algorithm (EWOA) [15], modified electric eel foraging optimizer [16], genetic algorithm (GA) [17], and adaptive fuzzy-neural network (AFNN) controller [18]. Despite the widespread use of PID controllers, its drawbacks—such as prolonged settling periods in high-inertia or delayed systems—underscore the necessity for more sophisticated and efficient control strategies to fulfill contemporary industrial demands for performance, sustainability, and cost-efficiency.

This study introduces a Proportional fractionalized Integral Derivative controller (PI$^{\alpha}$D) controller, marking its first documented application in electric furnace temperature regulation. The controller enhances performance by incorporating a fractional-order term into the integral gain [19-23], effectively mitigating the kick effect and improving the system's robustness against disturbances.The proposed PI$^{\alpha}$D extends the classical PID by adding a fractional-order integrator (α), resulting in four tunable parameters instead of three, while maintaining the same closed-loop structure. This additional flexibility allows for superior control accuracy in transient and frequency responses.

The principal contributions of this work are as follows:

(a) The HHO/ PI$^{\alpha}$D controller is proposed for the first time for electric furnace temperature control.

(b) A comparative study is conducted using the HHO algorithm to optimize various controllers, including classical PID, PIDA, and RPIDD².

(c) The robustness and adaptability of the proposed controller were tested in three different scenarios: (1) a step change in the desired temperature, (2) a step load disturbance, and (3) tracking a smooth random reference.

(d) Results show that the HHO/ PI$^{\alpha}$D controller outperforms classical methods in terms of overshoot, rise time, and settling time, confirming its effectiveness in precision thermal regulation.

The paper is organized as follows: Section 2 presents the temperature control system mathematical modelisation. Section 3 examines how the Harris Hawks Optimization (HHO) algorithm is incorporated into the design of the PI$^{\alpha}$D controller. Section 4 offers comprehensive simulation results, demonstrating the effectiveness of the proposed controller through detailed comparisons with existing approaches. Section 5 is dedicated to robustness analysis. Finally, Section 6 concludes the study and summarizes the key findings.

2. TEMPERATURE CONTROL SYSTEM MATHEMATICAL MODEL

The electric furnace system is composed of several essential components: the furnace chamber, a control unit, a temperature sensor (typically a thermocouple), a power regulator, and a heating coil. During operation, the sensor continuously monitors the internal temperature of the furnace and converts it into a voltage signal. This signal serves as negative feedback and is compared to a predefined reference value representing the target temperature. The resulting error is processed by the controller, which adjusts the power delivered to the heating element to reduce any temperature deviation.

Figure 1 presents the overall structure of the temperature control system, comprising the electric furnace, controller, thermocouple, and heater. The electric furnace temperature system transfer function $G_p(s)$ is represented in the s-domain as a second-order system with an accompanying time delay, as seen in Equation (1). The first-order Padé approach, as described in Equation (2), is used to estimate this delay. According to this approximation, the original transfer function in Equation (1) is restructured and presented in a revised version in Equation (3) [5, 15, 16, 24]. To better understand the dynamic behavior of the system, the open-loop step response is evaluated and presented in Figure 2.

$$G_p(s) = \frac{0.15}{s^2 + 1.1\,s + 0.2}\, e^{-1.5s} \tag{1}$$

$$e^{-1.5s} = \frac{1 - 0.75s}{1 + 0.75s} \tag{2}$$

$$G_p(s) = \frac{-0.1125s + 0.15}{0.75s^3 + 1.825s^2 + 1.25s + 0.2} \tag{3}$$

This response underlines the system's limitations: both the settling and rise times are excessively longer, and a significant steady-state error is evident—characterized as a difference between the reference input and the system output. For a unit step input of 1, the steady-state output attains just about 0.75. Table 1 highlights the principal performance indicators of the uncontrolled system, comprising settling time, rise time, and percentage overshoot.

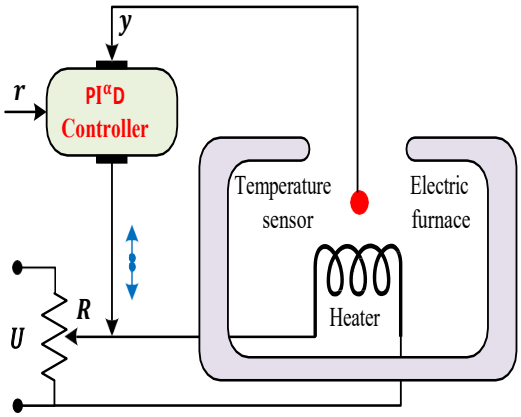

Figure 1. Schematic representation of electric furnace control.

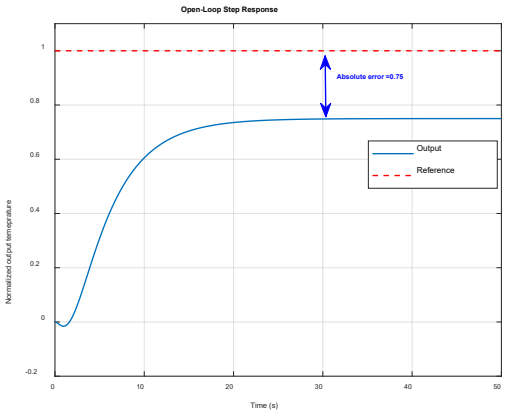

Figure 2. Step response of the system without the controller.

Table 1. Parameters measured without a controller.

Parameters	Values
Overshoot (%)	0.00
Settling time (s)	19.8
Rise time (s)	10.2

3. PROPOSED PI$^{\alpha}$D CONTROLLER BASED ON HHO ALGORITHM

3.1 Design of PI$^{\alpha}$D Controller

This study explores the implementation of a PI$^{\alpha}$D controller applied to the transfer function defined in Equation (3) for the temperature regulation of an electric furnace. The PI$^{\alpha}$D controller is justified in this study due to its enhanced degrees of freedom over traditional PID controllers. By incorporating a fractional-order element, the PI$^{\alpha}$D extends the number of tunable parameters from three to four, allowing for finer adjustment of the controller dynamics. This additional flexibility facilitates improved transient response, better frequency-domain behavior, and increased robustness against disturbances and nonlinearities typical of electric furnace temperature regulation. The fractional calculus element enables more precise modeling of system dynamics, especially for processes exhibiting memory and hereditary properties, making the PI$^{\alpha}$D well-suited for complex industrial systems where classical PID may fall short in performance and adaptability.

Figure 3 illustrates the operation of the furnace system within a PI$^{\alpha}$D feedback control loop, where $G_p(s)$ denotes the plant model and $G_c(s)$ the controller model. The controller regulates the system output $Y(s)$ in response to the reference input $R(s)$, ensuring stable performance even in the presence of external disturbances $D(s)$. The structure of a conventional PID controller is illustrated as:

$$G_c(s) = G_{PID}(s) = K_p + \frac{K_i}{s} + K_d s = \frac{K_d s^2 + K_p s + K_i}{s} \tag{4}$$

Incorporating fractional components into the control system modifies the conventional PID control rule by substituting the normal integral operator with its fractional equivalent $1/s$ [19, 20, 25]:

$$\frac{1}{s} = \frac{1}{s^{\alpha}} \cdot \frac{1}{s^{1-\alpha}} \tag{5}$$

Substituting Equation (5) into Equation (4) yields

$$G_{PI^{\alpha}D}(s) = \frac{K_d s^2 + K_p s + K_i}{s^{\alpha} s^{1-\alpha}} \tag{6}$$

where $0 < \alpha < 1$. Figure 4 shows the block diagram of PI$^{\alpha}$D controller.

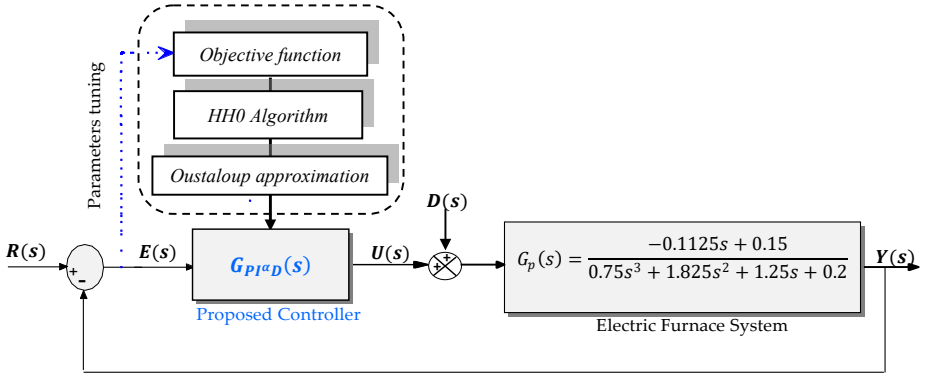

Figure 3. Proposed HHO based PI$^{\alpha}$D controller.

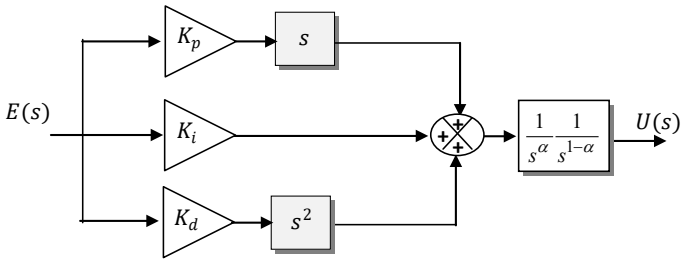

Figure 4. Block diagram of proposed PI$^{\alpha}$D controller.

3.2 Integral Absolute Error-Based Performance Criterion for PI$^{\alpha}$D Tuning Using HHO

This study employs the Integral Absolute Error (IAE) as the performance criterion for the HHO algorithm. The error signal $e(t)$ is computed by taking the difference between the reference model and the actual system response. A lower error number implies better approximation to the target controller settings.

$$J(K_p, K_i, K_d, \alpha) = IAE = \int_0^{t_{sim}} |e(t)|dt \tag{7}$$

The sign J denotes the performance index, which indicates how well the system output fits the reference model. The error signal $e(t)$ is defined as the difference between the reference and actual speed, i.e., $(v_{ref}(t) - v(t))$. In this investigation, the simulation length (t_{sim}) was set at 40 s.

3.3 HHO Algorithm

The nature-inspired population-based HHO algorithm (HHOA) [14] mimics Harris's Hawk hunting behaviour. It represents these hawks' hunting process mathematically. The distinct stages of the Harris Hawks formulation can be delineated into three primary phases as outlined in the following subsections.

3.3.1 The Exploration Stage

This represents the initial phase of the algorithm, where Harris Hawks utilize a wait-and-see strategy to apprehend their quarry by conducting arbitrary investigations in diverse areas.

$$X(t+1) = \begin{cases} X_{\text{rand}}(t) - r_1|X_{\text{rand}}(t) - 2r_2X(t)| & q \geq 0.5 \\ X_{\text{rabit}}(t) - X_m(t) - r_3(L_b + r_4(U_b - L_b)) & q < 0.5 \end{cases} \tag{8}$$

where $X(t+1)$ represents the Hawks' position in the subsequent iteration, $X_{\text{rabbit}}(t)$ indicates the rabbit's position, $X(t)$ denotes the vector indicating the current position of the hawks, (r_1, r_2, r_3, r_4) denote random numbers within the range of $(0,1)$, and (L_b, U_b) represent the variables of lower and upper bounds. Additionally, $X_{\text{rand}}(t)$ is a random hawk from the present position.

The mean of the Hawks' position is calculated as follows:

$$X_m(t) = \frac{1}{N}\sum_{i=1}^{N} X_i(t) \tag{9}$$

where X_m indicates the current Hawk population mean, and N is the entire Hawk population.

3.3.2 Transition from Exploration to Exploitation

This phase emulates various maneuvering tactics observed in Harris Hawks, which depend on the prey's flight energy. For instance, consider the energy level of a rabbit as an illustration of this behavior:

$$E = 2E_0\left(1 - \frac{t}{T_{\max}}\right) \tag{10}$$

where E represents the prey's escape energy, E_0 represents the initial energy and T_{max} represents the total number of iterations permitted.

3.3.3 The Exploitation Phase

The final phase of the HHO algorithm consists of four distinct strategies, each contingent upon the energy level of the prey and the likelihood of its escape. When considering $r < 0.5$ as indicative of the prey's successful escape chance and $r \geqslant 0.5$ as representing an unsuccessful escape attempt. In cases where $r \geqslant 0.5$ and $|E| \geq 0.5$, a soft besiege strategy will be executed, characterized by Equations (11) and (12).

$$X(t+1) = \Delta X(t) - E|X(t) - JX_{\text{rabbit}}| \tag{11}$$
$$\Delta X(t) = X_{\text{rabbit}}(t) - X(t) \tag{12}$$

where $\Delta X(t)$ represents the disparity between rabbit's location and current location at iteration t, J represents the magnitude of the rabbit's random. For $r \geqslant 0.5$ and $|E < 0.5|$, a severe besiege will be undertaken, as stated by Equation (13).

$$X(t+1) = X_{\text{rabbit}} - E|\Delta X(t)| \tag{13}$$

For $r < 0.5$ and $|E| \geq 0.5$, A mild besiege with gradual quick drive will be executed, as stated by Equations (14) and (15).

$$Y_1 = X_{\text{rabbit}} - E|X(t) - JX_{\text{rabbit}}| \tag{14}$$
$$Z_1 = Y_1 + S \times LF(D) \tag{15}$$

where D is the dimension of the problem, S is a $1 \times D$ random vector, and LF is the levy flight function. Therefore, Equation (16) fulfills the position update.

$$X(t+1) = \begin{cases} Y_1, & \text{if } F\big(X(t)\big) > F(Y_1) \\ Z_1, & \text{if } F\big(X(t)\big) > F(Z_1) \end{cases} \tag{16}$$

If both r and $|E|$ have values lower than a certain threshold, a hard besiege with increasing quick drive will be used, as described by Equations (17) – (19).

$$X(t+1) = \begin{cases} Y_2, & \text{if } F\big(X(t)\big) > F(Y_2) \\ Z_2, & \text{if } F\big(X(t)\big) > F(Z_2) \end{cases} \tag{17}$$

Y_2 and Z_2 are obtained using Equations (18) and (19), respectively.

$$Y_2 = X_{\text{rabbit}} - E|X(t) - JX_{\text{rabbit}}| \tag{18}$$
$$Z_2 = Y_2 + S \times LF(D) \tag{19}$$

The complete flowchart of the HHO algorithm is shown in Figure 5.

3.4 Method of Oustaloup Approximation

The estimation of the fractional-order (FO) integrator and differentiator is conducted through Oustaloup's approximation method [24]. The primary aim of Oustaloup's approximation [25] is to offer an estimation of a fractional operator.

$$G(s) = S^{\alpha}, \ (\alpha \in R) \tag{20}$$

The standard form of the Oustaloup filter is

$$G(s) = K\prod_{k=1}^{N}\frac{s + \omega_k^{'}}{s + \omega_k} \tag{21}$$

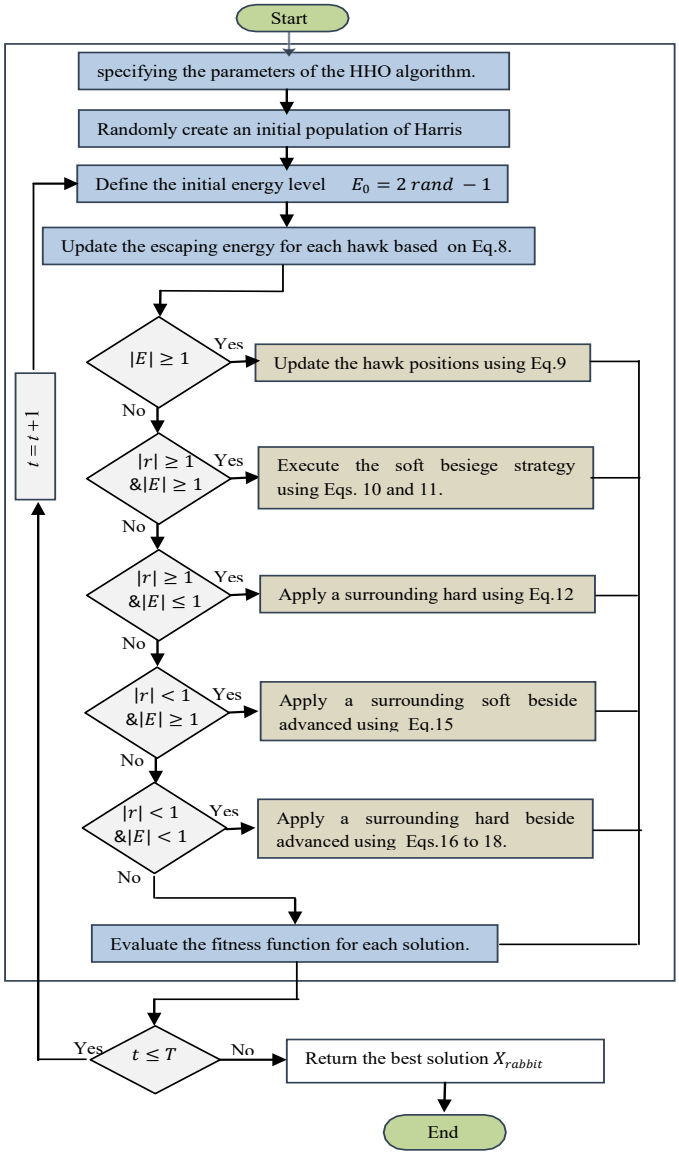

Figure 5. Schematic representation of the HHO algorithm.

The poles, zeros, and gain can be obtained from

$$\omega_k^{'} = \omega_b.\omega_u^{(2k-1-\gamma)/N}, \omega_k = \omega_b.\omega_u^{(2k-1+\gamma)/N}, \qquad K = \omega_h^{\gamma} \tag{22}$$

with, $\omega_u = \sqrt{\omega_h/\omega_b}$, for $k = 1,2,\ldots,N$. ω_h is the required frequency interval's upper, ω_b is the lower limits, N is the filter and γ is the derivative orders.

4. RESULTS AND DISCUSSION

The most suitable tuning settings for the PI$^{\alpha}$D controller were determined utilizing the HHO algorithm, based in a MATLAB/Simulink simulation model developed for electric furnace temperature management. Each Harris Hawk in the population signifies a proposed solution represented as a real-valued vector, which represents the controller's gains. The HHO technique was employed to determine the optimal values of the controller parameters for the system model $G_p(s)$, and the associated closed-loop transfer function was developed.

The transfer function of the PI$^{\alpha}$D controller is formulated using the proportional (K_p), integral (K_i), and derivative (K_d) gains, along with the fractional integral order α. The configuration of the HHO algorithm used to solve the optimization problem is as follows: the population size was set to 50 hawks, with a maximum of 40 iterations. The Lévy flight function constant was defined as 1.5. The search space for the controller parameters was constrained within specific bounds, with lower bounds set as $[0.01, 0.01, 0.01, 0.01]$ and upper bounds as $[5, 5, 5, 0.5]$ for $[K_p, K_i, K_d, \alpha]$. The dimensionality of the optimization problem was 4, and the simulation time for evaluating each candidate solution was set to 40 seconds. HHO algorithm was employed to design a PI$^{\alpha}$D controller for the system model $G_p(s)$ as shown in Equation (3), with the PI$^{\alpha}$D parameters set to $K_p = 3.2920$, $K_i = 0.6205$, $K_d = 4.3618$ and $\alpha = 48$.

The tuning procedures for the benchmark controllers (PID, PIDA, and RPIDD²) are aligned with methods commonly reported in recent studies on the same system. Specifically, the Modified Flower Pollination Algorithm (MOFPA) was employed to optimize the PID and PIDA controllers, while the Particle Swarm Optimization (PSO) algorithm was used for the RPIDD² controller. These choices ensure consistency with the literature and provide a fair basis of comparison.

The optimal HHO-PI$^{\alpha}$D, MOFPA-PID, MOFPA-PIDA and PSO-RPIDD^2 controllers for the electric furnace temperature control system as shown in Equations (23), (24), (25) and (26), respectively.

$$G_c(s)|_{\mathrm{PI}^{\alpha}\mathrm{D}} = \frac{4.36s^2 + 3.29\,s + 0.62}{s^{0.48}s^{0.52}} \tag{23}$$

$$G_c(s)|_{\mathrm{PID}} = 3.55 + \frac{0.61}{s} + 3.85\,s \tag{24}$$

$$G_c(s)|_{\mathrm{PIDA}} = 3.98 + \frac{0.66}{s} + 4.99\,s + 0.99\,s^2 \tag{25}$$

$$G_c(s)|_{\mathrm{RPIDD}^2} = 3.48 + \frac{0.65}{s} + 4.69\left(\frac{316.7752\,s}{s + 316.7752}\right) + 0.28\left(\frac{61.5626\,s}{s + 61.5626}\right)^2 \tag{26}$$

The resulting transfer function of the closed-loop system, which incorporates the proposed PI$^{\alpha}$D controller and unity feedback, is given by:

$$G_{CL\_\mathrm{PI}^{\alpha}\mathrm{D}}(s) = \frac{G_{HHO-\mathrm{PI}^{\alpha}\mathrm{D}}(s) * G_p(s)}{1 + G_{HHO-\mathrm{PI}^{\alpha}\mathrm{D}}(s) * G_p(s)} \tag{27}$$

Thus, the closed-loop transfer function corresponding to the HHO algorithm, combined with the proportional fractionalized integrator derivative controller, has been expressed in a fractional form. This fractionalization, detailed in Equation (27), incorporates an integrator of fractional order $\alpha = 0.48$. The value of α was obtained using the Oustaloup approximation method over a frequency range from $\omega_b = 0.1$ rad/s to $\omega_h = 10$ rad/s, under a unity feedback configuration given in Equation (28).

The obtained approximation is:

$$G_{HHO-\mathrm{PI}^{\alpha}\mathrm{D}}(s) = \frac{\begin{array}{c}-0.04907s^{13} - 1.254s^{12} - 12.29s^{11} - 58.6s^{10} - 141.8s^9 - \\ 144.9s^8 + 57.48s^7 + 317.5s^6 + 369.1s^5 + 225.9s^4 + \\ 81.22s^3 + 17.15s^2 + 1.959s + 0.09308\end{array}}{\begin{array}{c}0.7009s^{13} + 12.94s^{12} + 98.6s^{11} + 414.1s^{10} + \\ 1088s^9 + 1924s^8 + 2374s^7 + 2066s^6 + 1258s^5 + \\ 526.2s^4 + 146.8s^3 + 25.92s^2 + 2.606s + 0.1131\end{array}} \tag{28}$$

A comparison was conducted between the suggested PI$^{\alpha}$D controller, the standard PID controller, and alternative approaches such as PIDA and RPIDD², utilizing identical settings for an electric heating furnace. Standard MATLAB tools were employed to guarantee the reproducibility of results. Significant results are emphasized, with comprehensive analysis included in the following sections.

4.1 Transient Response Analysis

The likelihood of achieving improved system performance is affected by the choice of an appropriate goal function. To get the most out of the system's stability and dynamic responsiveness, this function is vital. This study aimed to achieve optimum system performance by using the IAE criteria as the objective function, as given in Equation (7). The closed-loop system employing the Proportional-Fractionalized Integral-Derivative (PID) control strategy, based in the HHO algorithm, demonstrates significant complexity (order 13; refer to Equation (28)). As a result, the total memory capacity of the proposed controller will be reduced to align more effectively with the corrective loop. As indicated in [19, 29], our present objective is to identify a low-order approximation of an integer-order model.

Figure 6 illustrates the error signal in model reduction, along with the original model where:

- $r(t)$: the input signal (reference signal) applied to both the original model and the reduced model.
- $G(s)$: the transfer function of the original high-order system.
- $y(t)$: Output of the original system $G(s)$.
- $G_{r/m}(s)$: Transfer function of the reduced-order model, designed to approximate $G(s)$ with lower complexity.
- $\hat{y}(t)$: Output of the reduced-order model $G_{r/m}(s)$.
- $e(t) = y(t) - \hat{y}(t)$: Error signal defined as the difference between the original and the reduced model output.

This block diagram represents a model order reduction framework, where a high-order system is approximated by a reduced-order system.

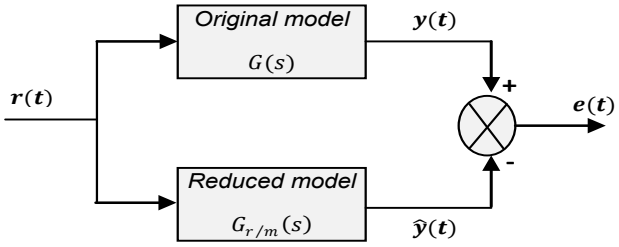

Figure 6. Error signal for model reduction.

$$G(s) = \frac{b_1 s^{n-1} + \cdots + b_{n-1}s + b_0}{s^n + a_1 s^{n-1} + \cdots + \alpha_{n-1}s + a_n} \tag{29}$$

As noted in [19, 29], our current goal is to find a low-order approximation of an integer-order model.

$$G_{r/m}(s) = \frac{\beta_1 \mathrm{s}^{\mathrm{r}} + \cdots + \beta_r s + \beta_{r+1}}{\mathrm{s}^m + \alpha_1 s^{m-1} + \cdots + \alpha_{m-1}s + \alpha_m} \tag{30}$$

The Laplace transform of the error signal can be expressed as:

$$E(s) = G(s) - G_{r/m}(s) \tag{31}$$

where $R(s)$ represents the Laplace transform of the input signal $r(t)$. The objective function for minimizing the H_2-norm of the reduction error signal is given by:

$$J = \min_{\theta} \left\| \hat{G}(s) - G_{r/m}(s) \right\|_2 \tag{32}$$

where J is the performance criterion, $G_{r/m}(s)$ is the reduced-order model and θ represents the parameters that are adjusted to ensure that:

$$\theta = [\beta_1, \ldots, \beta_r, \alpha_1, \ldots, \alpha_m] \tag{33}$$

Equation (34) presents the low-order closed-loop transfer function associated with the high-order closed-loop system described in Equation (28).

$$G_{CL\_RO\_\mathrm{PI}^{\alpha}\mathrm{D}}(s) = \frac{-5.981s^3 + 5.212s^2 + 6.781\mathrm{s} + 6.648 \times 10^{-10}}{s^5 + 9.684s^4 + 21.18s^3 + 23.21s^2 + 8.238s + 8.077 \times 10^{-10}} \tag{34}$$

To evaluate the accuracy of the reduced-order PI$^{\alpha}$D controller, both time-domain and frequency-domain comparisons were performed. The results are presented in Figures 7 and 8.

In the time-domain evaluation, the reduced-order PI$^{\alpha}$D controller exhibits a step response that closely aligns with that of the original high-order controller. As illustrated in Figure 7, both systems demonstrate nearly identical rise time, overshoot, and settling time, indicating that the model reduction has minimal impact on transient performance. In the frequency domain, Figure 8 shows that the magnitude and phase responses of the reduced and original controllers are highly consistent across the examined frequency range. This confirms that the essential dynamic behavior is well preserved after model reduction. Overall, the reduced-order PI$^{\alpha}$D controller offers an accurate approximation of the original system, maintaining control performance while significantly lowering computational complexity, making it well suited for real-time implementation.

Figure 9 depicts the system's response to input changes under the control of the proposed PI$^{\alpha}$D controller, in comparison with other controllers including the classical MOFPA-PID, MOFPA-PIDA, and PSO-RPIDD^2 controllers. The main plot demonstrates that all controllers achieve steady-state convergence; however, noticeable differences arise in transient performance. The zoomed-in view highlights the superior performance of the proposed PI$^{\alpha}$D controller, which exhibits, shorter rise time (T_r), faster settling time (T_s), minimal overshoot (OS), and reduced oscillations compared to the other controllers. These improvements confirm the efficacy of the fractional-order dynamics in enhancing control precision and robustness during the critical initial response phase. Table 2 presents the transient response metrics of the four controllers, including measures such as the maximum overshoot, rising time (measured from 10% to 90%), settling time (within a tolerance of ±2%), and peak time.

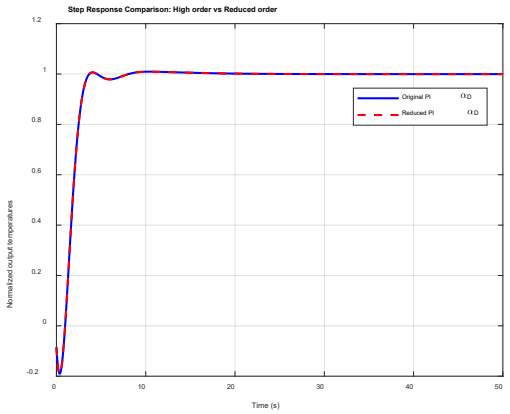

Figure 7. Step response of original and reduced PI$^{\alpha}$D controllers.

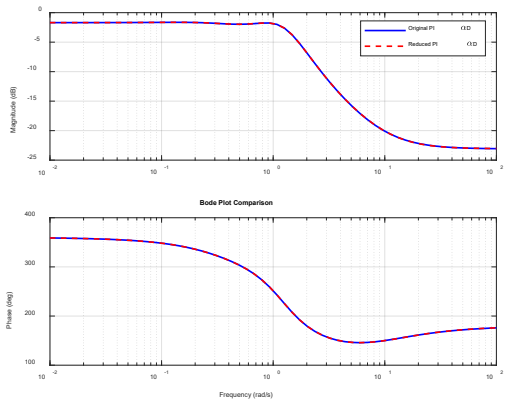

Figure 8. Bode plot of original and reduced PI$^{\alpha}$D controllers.

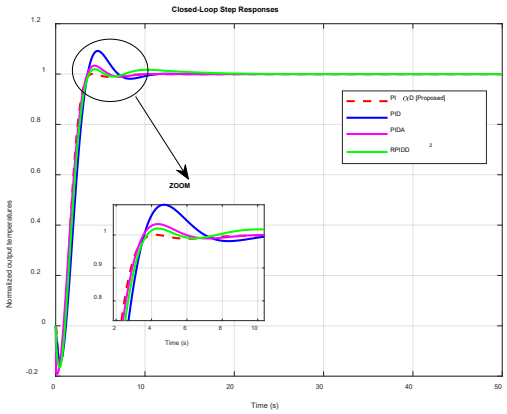

Figure 9. Input tracking performance with various controllers.

Table 2. Comparative analysis of the transient response.

Controllers	T_r (s)	T_s (s)	OS (%)	T_p (s)
HHO-PI$^{\alpha}$D [Proposed]	1.6549	3.4335	0.1169	4.1836
MOFPA-PID	1.7818	6.4827	9.1687	4.7397
MOFPA-PIDA	1.8368	5.1277	3.3096	4.3534
PSO-RPIDD^2	1.7933	3.5218	1.9579	4.3715

As can be seen from Table 2, the proposed HHO-PI$^{\alpha}$D controller outperforms the others by achieving the fastest rise time (1.6549 s), the shortest settling time (3.4335 s), and the lowest overshoot (0.1169%), demonstrating superior stability and responsiveness. In comparison, the classical PID controller shows moderate performance, while the MOFPA|-PIDA and PSO-RPIDD² controllers exhibit slower dynamics and higher overshoot, making them less effective. Overall, the proposed HHO-PI$^{\alpha}$D controller delivers the best transient performance among all the controllers evaluated.

4.2 Frequency Response Analysis

Figure 10 shows the Bode plot comparison of the open loop transfer function for the four controllers: the proposed PI$^{\alpha}$D, classical PID, PIDA, and RPIDD². Table 3 summarizes the frequency-domain performance of the controllers, including gain margin G_m, phase margin φ_m, and bandwidth Bw . Higher gain and phase margins indicate improved stability and robustness, while a larger bandwidth reflects a faster dynamic response.

As can be seen from Figure 10, the proposed HHO-PI$^{\alpha}$D controller (red dashed line) demonstrates a higher gain in the low-frequency range and a smoother phase transition, indicating enhanced robustness and effective disturbance rejection. In contrast, the MOFDA-PID and MOFDA-PIDA controllers show steeper gain roll-off and more abrupt phase drops, which may limit their stability margins. The PSO-RPIDD² controller exhibits a broader bandwidth but may introduce sensitivity at high frequencies. Overall, the HHO-PI$^{\alpha}$D controller provides a well-balanced compromise between stability, robustness, and frequency-domain performance.

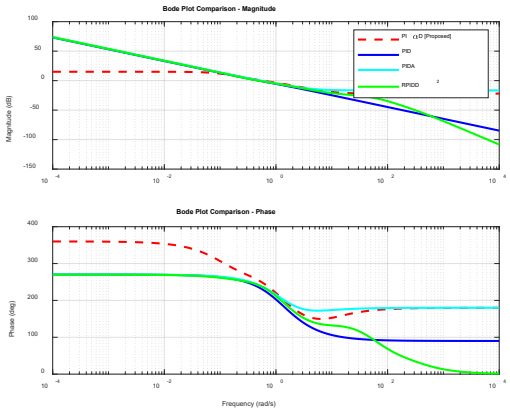

Figure. 10 Bode plots comparison for different controller designs.

Table 3. Frequency domain stability metrics.

Controllers	G_m (dB)	φ_m (degree)	Bw (rad/s)
HHO-PI$^{\alpha}$D [Proposed]	8.3685	67.991	1.6463
MOFPA-PID	8.5259	55.588	1.3057
MOFPA-PIDA	11.262	59.163	1.4069
PSO-RPIDD^2	8.8077	61.834	1.4713

As shown in the Table 3, the proposed HHO-PI$^{\alpha}$D controller demonstrates the best overall trade-off, combining a high gain margin, a large phase margin, and the highest bandwidth, indicating strong robustness and fast dynamic response. Although the classical MOFPA-PID controller achieves a slightly higher gain margin, it exhibits lower phase margin and bandwidth. The MOFPA-PIDA controller performs the weakest, with the lowest gain margin and bandwidth, reflecting limited stability and responsiveness. The PSO-RPIDD² controller provides the highest phase margin but shows reduced gain robustness compared to the proposed approach.

4.3 Comparison of Different Error Criteria

In PID controller design, the fitness function is often based on the amount of deviation that exists between the output of the system and the value that is intended. Criteria that are based on common errors: Integral-Absolute-Error (IAE), Integral-Squared-Error (ISE), Integral-Time-weighted-Absolute-Error (ITAE), and Integral-Time-weighted-Squared-Error (ITSE) are used to evaluate and optimize performance, each emphasizing different aspects of the system's transient response. The criteria are given in Equations (35)-(38) where $e(t)$ denotes the deviation between the target output and the measured output at time t. While minimizing these criteria can reduce overshoot, it may increase settling time. Table 4 presents the values of the four standard performance indices IAE, ISE, ITAE, and ITSE for all controllers.

$$ISE = \int e(t)^2 \cdot dt \tag{35}$$

$$IAE = \int |e(t)| \cdot dt \tag{36}$$

$$ITAE = \int t \cdot |e(t)| dt \tag{37}$$

$$ITSE = \int t \cdot [e(t)^2] \cdot dt \tag{38}$$

Table 4. Performance evaluation based on ITAE, ITSE, IAE, and ISE criteria.

Controllers	IAE	ISE	ITAE	ITSE
HHO-PI$^{\alpha}$D [Proposed]	2.0686	1.7729	2.8166	1.4278
MOFPA-PID	2.5624	2.0889	4.1218	2.0243
MOFPA-PIDA	2.1045	1.7793	2.521	1.3854
PSO-RPIDD^2	2.3371	1.9449	4.1084	1.6773

Table 4 shows that the proposed HHO-PI$^{\alpha}$D controller achieves the lowest values of IAE (2.0686) and ISE (1.7729), highlighting its effectiveness in minimizing overall error magnitude and energy. However, the MOFPA-PIDA controller shows superior performance in terms of ITAE (2.521) and ITSE (1.3854), indicating faster attenuation of errors over time and improved suppression of late-stage deviations. This suggests that while the HHO-PI$^{\alpha}$D controller ensures strong general tracking performance, the MOFPA-PIDA controller is more effective in scenarios requiring rapid stabilization and reduced long-term error impact.

5. Robustness Analysis

This section analyzes three distinct scenarios:

Scenario 1: Tracking performance under a step change in desired temperature.
In this scenario, the system is subjected to a step change in the desired temperature to evaluate its response. At $t = 20$ s, a step change of 0.5 is applied. Figure 11 shows the step response of the system using four controllers: PI$^{\alpha}$D, PID, PIDA, and RPIDD^2. A reference step change is applied at $t = 20$ s. The PI$^{\alpha}$D and RPIDD^2 controllers show better performance compared to PID and PIDA, with faster settling time and lower overshoot. The zoomed views highlight the transient behavior before and after the step change. The proposed PI$^{\alpha}$D and RPIDD^2 controllers closely follow the reference and recover quickly from disturbances, while the PID controller has the highest overshoot. These results confirm that the PI$^{\alpha}$D and RPIDD^2 controllers provide improved tracking and stability.

Table 5 indicates the performance in this case. The proposed HHO-PI$^{\alpha}$D controller achieved the best performance in the reference tracking scenario, with zero overshoot, the fastest rise time, and the shortest settling time compared to MOFPA-PID, MOFPA-PIDA, and PSO-RPIDD^2 controllers.

Table 5. Performance metrics for reference tracking (step change at $t = 20$ s).

Controllers	T_r (s)	T_s (s)	OS (%)	T_p (s)
HHO-PI$^{\alpha}$D [Proposed]	20.950	23.073	0.0000	4.1836
MOFPA-PID	21.117	25.678	3.0555	4.7397
MOFPA-PIDA	21.103	23.107	1.1023	4.3534
PSO-RPIDD^2	21.063	23.233	0.68113	4.3715

Scenario 2: Impact of a step load variation on system stability
This scenario investigates the effect of a sudden load disturbance on the system's performance, as illustrated in Figure 12, the system was subjected to a step load disturbance introduced at t = 30 s. Figure 13 illustrates the system's response under the four different controllers.

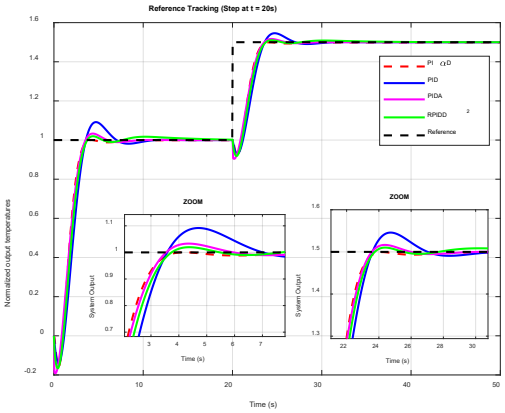

Figure 11. Dynamic response of the system in scenario 1.

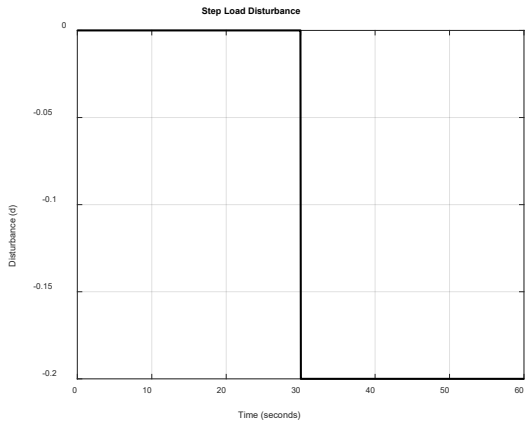

Figure 12. Step disturbance.

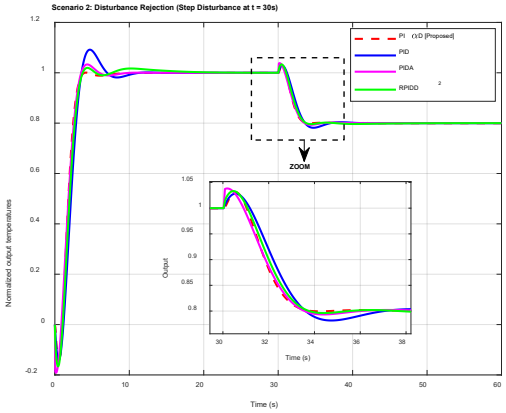

Figure 13. Dynamic response of the system in scenario 2.

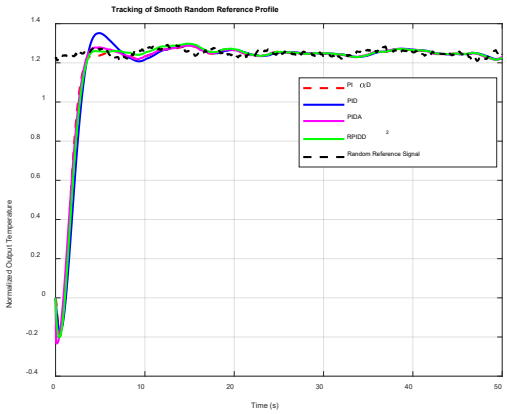

Figure 14. Output response of controllers under a smooth random temperature reference.

In Figure 13, before the disturbance, all controllers track the reference accurately. At the disturbance moment, the system output drops and then recovers. A zoomed-in view (30-38 s) highlights the difference in disturbance rejection performance. The proposed PI$^{\alpha}$D controller shows the fastest and smoothest recovery with minimal overshoot and fast return to steady state. RPIDD^2 controller also performs well, closely following the proposed controller. In contrast, the PID and PIDA controllers have slower recovery and more oscillations. This result confirms that the PI$^{\alpha}$D controller is more robust to sudden disturbances, making it more suitable for dynamic environments where load changes occur.

Scenario 3: Smooth random reference tracking test

To assess tracking performance under realistic conditions, a smooth random reference signal ranging from 1.0 to 1.5 was generated to emulate gradual temperature changes in an industrial furnace. To evaluate tracking quality, the following performance indices were computed: IAE, ISE, ITAE, and ITSE.

Figure 14 illustrates the tracking performance of each controller in response to the smooth, randomly varying reference signal. Table 6 summarizes the values of four standard performance indices computed for each controller. These indices provide a comprehensive evaluation of tracking accuracy and robustness, with each emphasizing different aspects such as total error, large deviations, and time-weighted penalties. The results demonstrate that the proposed PI$^{\alpha}$D and RPIDD^2 controllers outperform conventional PID and PIDA in all tracking metrics. Their ability to follow a dynamic reference with minimal delay and error highlights their robustness and adaptability for real-world furnace control applications. Table 6 shows that the HHO-PI$^{\alpha}$D controller achieved excellent tracking performance, with error values close to the best-performing PSO-RPIDD^2 controller. This confirms the strong ability of HHO-PI$^{\alpha}$D to handle dynamic reference changes. In contrast, the classical PID controller exhibited the highest errors, indicating limited effectiveness in tracking varying signals.

The tracking performance analysis under a smooth, random reference signal showed that advanced controllers, particularly PI$^{\alpha}$D and PIDA, outperformed classical PID. PI$^{\alpha}$D achieved excellent accuracy (low IAE and ITAE), while PIDA minimized late errors (lowest ITSE), both demonstrating strong suitability for realistic thermal control scenarios. RPIDD^2 provided a moderate improvement over PID, which exhibited the highest error values across all indices. These results highlight the effectiveness of fractional and derivative-augmented controllers in industrial furnace temperature regulation.

Table 6. Performance indices for random reference tracking.

Controllers	IAE	ISE	ITAE	ITSE
HHO-PI$^{\alpha}$D [Proposed]	3.2432	2.7072	20.057	2.5976
MOFPA-PID	3.8203	3.1877	22.990	3.5454
MOFPA-PIDA	3.2231	2.7126	20.132	2.5217
PSO-RPIDD^2	3.4127	2.9667	20.777	2.9768

6. CONCLUSION

In this study, a Proportional Fractionalized Integral Derivative (PI$^{\alpha}$D) controller was proposed for regulating temperature in electric furnaces. The controller has proportional, fractionalized integral and derivative, components. Its parameters were optimized using the HHO method using the IAE criteria. Effectiveness of the PI$^{\alpha}$D controller was tested by comparing it to other standard integer-order PID controllers, PIDA, and RPIDD^2. The comparisons showed the significant potential of the suggested controller for high-performance industrial applications. In the time-domain study, the PI$^{\alpha}$D method produced better results, showing faster rise and settling times, less overshoot, and shorter peak periods. In the frequency domain, it showed outstanding strength and stability, with unlimited phase margins, high gain margins, and wider bandwidths outperforming current controllers in many quality aspects and indicating major improvements in controlling furnace temperature. This study also highlighted additional opportunities for more investigation. Evaluating the proposed method's adaptability and efficacy in real-world industrial contexts may provide more insights. Furthermore, analyzing the influence of environmental uncertainty

on the system may enhance its robustness. Future research should examine the effects of the approximation method used on controller design.

ACKNOWLEDGMENT AND FUNDING

The authors acknowledge all the concerned who support this work. The authors receive no financial support for the research, authorship, and publication of this article.

DECLARATION OF CONFLICTING INTERESTS

The authors declare no potential conflicts of interest with respect to the research and publication of this article.

REFERENCES

[1] J. W. Li, C. F. Yan and J. Liu, Design of temperature control system based on fuzzy PID, *Advanced Materials Research*, 418, 2012, 1756-1759.

[2] T. Sheng, H. Luo and M. Wu, Design and simulation of a multi-channel biomass hot air furnace with an intelligent temperature control system, *Agriculture*, 14(3), 2024, 419.

[3] E. Grassi and K. Tsakalis, PID controller tuning by frequency loop-shaping: Application to diffusion furnace temperature control, *IEEE Transactions on Control Systems Technology*, 8(5), 2000, 842-847.

[4] D. Ajorloo, M. Nazari, N. Sepehry and A. Mohammadzadeh, Mathematical modeling and designing an optimized fuzzy temperature controller for a vacuum box electric furnace: Numerical and experimental study, *Transactions of the Institute of Measurement and Control*, 45(7), 2023, 1193-1212.

[5] N. Pringsakul and D. Puangdownreong, MOFPA-based PIDA controller design optimization for electric furnace temperature control system, *International Journal of Innovative Computing, Information and Control*, 16(6), 2020, 1863-1876.

[6] L. Liu, D. Xue and S. Zhang, General type industrial temperature system control based on fuzzy fractional-order PID controller, *Complex & Intelligent Systems*, 9(3), 2023, 2585-2597.

[7] K. Rsetam, M. Al-Rawi and Z. Cao, Robust adaptive active disturbance rejection control of an electric furnace using additional continuous sliding mode component, *ISA Transactions*, 130, 2022, 152-162.

[8] G. C. Goodwin, R. H. Middleton, M. M. Seron and B. Campos, Application of nonlinear model predictive control to an industrial induction heating furnace, *Annual Reviews in Control*, 37(2), 2013, 271-277.

[9] R. Valarmathi, P. R. Theerthagiri, S. Rakeshkumar and V. Gomathi, Design of genetic algorithm based internal model controller for a heat exchanger, *Proceedings of the International Conference on Computation of Power, Energy, Information and Communication (ICCPEIC)*, Chennai, India, 2018, 489-495.

[10] A. Jayachitra and R. Vinodha, Genetic algorithm based PID controller tuning approach for continuous stirred tank reactor, *Advances in Artificial Intelligence*, 2014(1), 2014, 791230.

[11] V. Sinlapakun and W. Assawinchaichote, Optimized PID controller design for electric furnace temperature systems with Nelder-Mead algorithm, *Proceedings of the 12th International Conference on Electrical Engineering/Electronics, Computer, Telecommunications and Information Technology (ECTI-CON)*, Hua Hin, Thailand, 2015, 1-4.

[12] W. Jiang and X. Jiang, Design of an intelligent temperature control system based on the fuzzy self-tuning PID, *Procedia Engineering*, 43, 2012, 307-311.

[13] R. Zhang, Q. Zou, Z. Cao and F. Gao, Design of fractional order modeling based extended non-minimal state space MPC for temperature in an industrial electric heating furnace, *Journal of Process Control*, 56, 2017, 13-22.

[14] H. Liang, Z. K. Sang, Y. Z. Wu, Y. H. Zhang and R. Zhao, High precision temperature control performance of a PID neural network-controlled heater under complex outdoor conditions, *Applied Thermal Engineering*, 195, 2021, 117234.

[15] M. M. Hussein, S. Alkhalaf, T. H. Mohamed, D. S. Osheba, M. Ahmed, A. Hemeida and A. M. Hassan, Modern temperature control of electric furnace in industrial applications based on modified optimization technique, *Energies*, 15(22), 2022, 8474.

[16] S. A. Alzakari, D. Izci, S. Ekinci, A. A. Alhussan and F. A. Hashim, A new control scheme for temperature adjustment of electric furnaces using a novel modified electric eel foraging optimizer, *AIMS Mathematics*, 9(5), 2024, 13410-13438.

[17] I. Chew, F. Wong, A. Bono, J. Nandong and K. Wong, Genetic algorithm optimization analysis for temperature control system using cascade control loop model, *International Journal of Computing and Digital Systems*, 9(1), 2020, 119-128.

[18] V. D. Phan, X. H. Nguyen, V. N. Dinh, T. S. Dang, V. C. Le, S. P. Ho, H. C. Ta, D. T. Duong and T. A. Mai, Development of an adaptive fuzzy-neural controller for temperature control in a brick tunnel kiln, *Electronics*, 13(2), 2024, 342.

[19] A. Idir, Y. Bensafia, K. Khettab and L. Canale, Performance improvement of aircraft pitch angle control using a new reduced order fractionalized PID controller, *Asian Journal of Control*, 25(4), 2023, 2588-2603.

[20] A. Idir, Y. Bensafia and L. Canale, Influence of approximation methods on the design of the novel low-order fractionalized PID controller for aircraft system, *Journal of the Brazilian Society of Mechanical Sciences and Engineering*, 46(2), 2024, 98.

[21] A. Idir, H. Akroum, S. A. Tadjer and L. Canale, A comparative study of integer order PID, fractionalized order PID and fractional order PID controllers on a class of stable system, *Proceedings of the IEEE International Conference on Environment and Electrical Engineering and Industrial and Commercial Power Systems Europe (EEEIC/I&CPS Europe)*, Madrid, Spain, 2023, 1-6.

[22] S. Guedida, B. Tabbache, K. Nounou and A. Idir, Reduced-order fractionalized controller for disturbance compensation based on direct torque control of DSIM with less harmonic, *Electrica*, 24(2), 2024, 450-462.

[23] Z. Ousaadi, H. Akroum and A. Idir, Robustness enhancement of fractionalized order proportional integral controller for speed control of indirect field-oriented control induction motor, *Przegląd Elektrotechniczny*, 2024(3), 2024, 166-171.
[24] M. M. Gani, M. S. Islam and M. A. Ullah, Optimal PID tuning for controlling the temperature of electric furnace by genetic algorithm, *SN Applied Sciences*, 1, 2019, 880.
[25] Y. Bensafia, K. Khettab and A. Idir, A novel fractionalized PID controller using the sub-optimal approximation of FOTF, *Algerian Journal of Signals and Systems*, 7(1), 2022, 21-26.
[26] A. A. Heidari, S. Mirjalili, H. Faris, I. Aljarah, M. Mafarja and H. Chen, Harris hawks optimization: Algorithm and applications, *Future Generation Computer Systems*, 97, 2019, 849-872.
[27] Y. Bensafia, K. Khettab and A. Idir, An improved robust fractionalized PID controller for a class of fractional-order systems with measurement noise, *International Journal of Intelligent Engineering and Systems*, 11(2), 2018, 200-207.
[28] A. Oustaloup, F. Levron, B. Mathieu and F. M. Nanot, Frequency-band complex noninteger differentiator: Characterization and synthesis, *IEEE Transactions on Circuits and Systems I: Fundamental Theory and Applications*, 47(1), 2000, 25-39.
[29] D. Xue and Y. Chen, Sub-optimum H_2 rational approximations to fractional order linear systems, *Proceedings of the ASME International Design Engineering Technical Conferences and Computers and Information in Engineering Conference (IDETC/CIE)*, Long Beach, USA, 2005, 1527-1536.
[30] W. Zhao, L. Wang, Z. Zhang, H. Fan, J. Zhang, S. Mirjalili, N. Khodadadi and Q. Cao, Electric eel foraging optimization: A new bio-inspired optimizer for engineering applications, *Expert Systems with Applications*, 238, 2024, 122200.
[31] S. Mirjalili and A. Lewis, The whale optimization algorithm, *Advances in Engineering Software*, 95, 2016, 51-67.